Research Square

Preprints are preliminary reports that have not undergone peer review.
They should not be considered conclusive, used to inform clinical practice,
or referenced by the media as validated information.

Dual-Layer Optimization for H2-NH3 Integrated Energy System

Danxi Liang
North China Electric Power University
Jie Song
North China Electric Power University
Zheng Zong
China Electric Power Research Institute Co., Ltd
YanMin Zu
China Electric Power Research Institute Co., Ltd
GuiZhi Xu
North China Electric Power University
MengYuan Yang
China Electric Power Research Institute Co., Ltd
YuTing Zhu
China Electric Power Research Institute Co., Ltd
Kun Hou
China Electric Power Research Institute Co., Ltd
YongSheng Zhang
yszhang@ncepu.edu.cn

North China Electric Power University

Research Article

Keywords: integrated energy system, thermal power units, combined-heat-and-power(CHP), dual-layer optimization model

Posted Date: September 11th, 2026

DOI: https://doi.org/10.21203/rs.3.rs-7323077/v1

License: This work is licensed under a Creative Commons Attribution 4.0 International License.
Read Full License

Additional Declarations: No competing interests reported.

Dual-Layer Optimization for H_2-NH_3 Integrated Energy System

Danxi Liang[1,2],Jie Song[1,2],Zheng Zong[2] ,YanMin Zu[2],GuiZhi Xu[1,2] ,MengYuan Yang[2],YuTing Zhu[2] , Kun Hou[2],YongSheng Zhang[1]

1. School of Energy, Power and Mechanical Engineering, North China Electric Power University, Beijing
2. China Electric Power Research Institute Co., Ltd., Beijing

*Corresponding Author: YongSheng Zhang Email: yszhang@ncepu.edu.cn

Abstract—In the high penetration rate of wind solar integrated energy systems, the problem of energy waste has become increasingly prominent. This article proposes an innovative technical solution of co combustion of ammonia doped thermal power units and electric to ammonia conversion. This method can not only improve the utilization rate of wind solar resources, but also optimize the environmental protection and safety of the energy system. Firstly, this article designs a new configuration that couples electric to ammonia conversion with integrated energy systems, and constructs coordinated operation indicators for wind solar thermal ammonia systems to comprehensively evaluate the wind solar power consumption status, the output of thermal power units, as well as the economic benefits and stability of electric to ammonia conversion operation. Then, a dual-layer optimization model was constructed, where the first layer objective is to maximize the coordinated operation indicators, and the second layer objective is to minimize the operating costs of the electric to ammonia and fire wind solar integrated energy systems. By comparing and analyzing various models in different scenarios in a certain region of Inner Mongolia, the effectiveness of the models is verified. Research analysis shows that, taking typical daily scenarios as an example, there is a significant difference between using this model and not using it in winter and summer, respectively. The use of this model significantly reduces the system cost, with further reductions of 4.4% and 5.41%, respectively. The safety and stability of thermal power units have been significantly improved, and carbon emissions have also been reduced to varying degrees.

Keywords—integrated energy system,thermal power units,combined-heat-and-power(CHP),dual-layer optimization model.

1 Introduction

In recent years, renewable energy generation technologies, particularly photovoltaic and wind power, have experienced rapid development and widespread adoption both domestically and internationally. However, the inherent fluctuations and intermittency in the power output of these sources limit their further development. To ensure good economy and stability in power systems, it is often necessary to deploy large-capacity energy storage devices.Numerous scholars worldwide have conducted detailed research on the optimized scheduling of integrated energy systems (IES) incorporating energy storage. For instance:Some studies propose using battery energy storage systems (BESS) to achieve peak shaving and valley filling, aiding thermal power units in performing deep peak regulation[1].Research has demonstrated the use of compressed air energy storage (CAES) technology to mitigate the intermittency and volatility issues associated with renewable energy generation[2].Additionally,studies have specifically explored utilizing hydropower plants to absorb wind power generation and photovoltaic power generation, thereby optimizing grid operational stability[3].Despite this progress, the practical application of these solutions still faces difficulties. For example, both chemical and physical energy storage technologies, such as batteries, grapple with technical challenges related to cost and capacity limitations. Therefore, there is an urgent need for the emergence of novel energy storage technologies to meet the requirements of engineering projects.

Hydrogen, as a clean energy source, possesses significant energy storage potential and high energy density. Power-to-hydrogen (P2H) technology achieves energy storage by producing hydrogen through water electrolysis[4]. However, due to hydrogen's physical properties—particularly its low density—its transportation and storage require stringent conditions, typically under high pressure (30–70 MPa) or at cryogenic temperatures (-250°C). This process not only incurs energy losses of 15%–40%[5] but also faces major barriers to large-scale adoption, including the stringent requirements for extreme conditions and potential leakage risks[6].To address these limitations of hydrogen in large-scale energy storage applications, literature[7] proposes using ammonia as an energy storage medium.

Ammonia, with a calorific value of 18.72 MJ/kg comparable to conventional coal, serves as a zero-carbon energy carrier. Compared to hydrogen, ammonia offers superior economic and safety performance in transportation and storage due to its milder liquefaction conditions (0.9 MPa or -33°C). Power-to-ammonia (P2A) technology produces hydrogen via water electrolysis, followed by catalytic synthesis into ammonia. Ammonia's chemical stability effectively addresses hydrogen's instability issues.While current research predominantly focuses on power-to-hydrogen applications, literature[8] specifically analyzes the energy consumption of P2A technology. Studies comparing the production and storage costs of hydrogen, ammonia, and methanol derived from green hydrogen reveal ammonia as the most cost-effective option—31% and 18% lower than hydrogen and methanol, respectively[9].Under carbon neutrality policies, recent proposals for ammonia co-firing in thermal power units aim to accelerate progress toward dual-carbon goals. This approach holds significant promise for decarbonizing China's coal-dominated energy structure. Thermodynamic calculations further confirm the feasibility of reducing carbon emissions through ammonia co-firing in large-scale coal-fired boilers[10].

Most researchers currently focus on power-to-ammonia or ammonia combustion, rarely analyzing the entire-ammonia manufacturing process combined with renewable energy across multiple dimensions. Many issues in these individual research areas remain unresolved. Consequently, this paper proposes a dual-layer optimal scheduling model comparing power-to-ammonia with ammonia cofiring. The model integrates a thermal-wind-solar comprehensive energy system.Firstly, it analyzes the power-to-ammonia system, and secondly, it examines the thermal-wind-solar comprehensive system. Finally, a dual-layer optimization model is established. The first layer aims to maximize coordinated operation indicators, while the second layer strives to minimize the operating costs of the power-to-ammonia integrated thermal-wind-solar system.

This paper uses typical data from a site in Ordos, Inner Mongolia, applies it to the proposed model, and employs Matlab/Simulink simulations. The aim is to explore the impact of power-to-ammonia and ammonia cofiring technologies on thermal-wind-solar systems and to verify the dual-layer scheduling optimization model's effectiveness.

2 Configuration of Power-to-Ammononia Coupled Thermal-Wind-Solar Integrated Energy System

Fig.1 illustrates the basic structure of power-to-hydrogen-to-ammonia integrated with a thermal-wind-solar hybrid energy system. In this model, photovoltaic, wind-turbine,thermal, and combined-heat-and-power (CHP) plants jointly meet the electric load. The heat load is supplied by the ammonia plant and CHP plant. The core of the power-to-ammonia system is water electrolysis for hydrogen production.

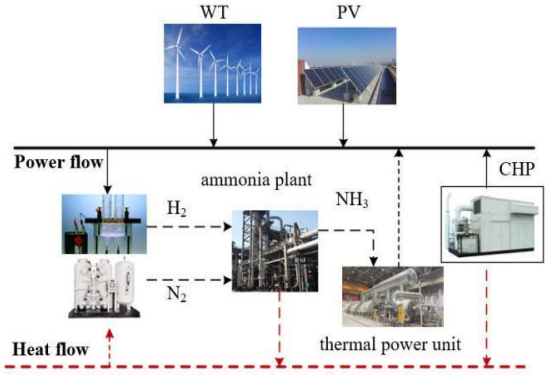


Fig. 1. Configuration of Electric Ammonia Production System Coupled with Thermal-Wind-Solar Integrated Energy System

In In Fig.1, wind turbines and photovoltaic systems supply electricity to the power grid, and then ammonia is synthesized for use by thermal power units. The heat generated during ammonia synthesis at the ammonia plant[11] is included in the heat load and is considered as one of the sources of thermal power. The thermal power is calculated as follows:

$$W_t^{ECA} = \eta^{ECA} \sigma m_t^{ECA,NH_3} \tag{1}$$

In the formula: W_t^{ECA} is the heat power supplied by the power-to-ammonia system to the entire system during period t; η^{ECA} is the heat release ratio for heat supply; m_t^{ECA,NH_3} is the mass of ammonia produced by the power-to-ammonia process during period t; σ is the heat power released per unit of NH_3.

Upon integrating the electric ammonia production system into the power grid, the power output from wind power generation and photovoltaic power generation follows two pathways:A portion is fed into the grid;The remainder supplies the electric ammonia production system.Achieving both economic and environmental objectives for the entire system necessitates coordinated operation among all components, which constitutes the core challenge of this system model.

3 Dual-Layer Optimal Scheduling of Power-to-Ammonia Coupled Thermal-Wind-Solar Hybrid Energy Systems

3.1 Grid-Connected Mode Control

This study addresses the coordinated operation of microgrid components in an integrated system for hydrogen production via water electrolysis and subsequent ammonia synthesis, coupled with a thermal-wind-solar integrated energy system. We focus on optimizing the combined heat-power dispatch, constructing a dual-layer optimization model whose structure is illustrated in Fig. 2.

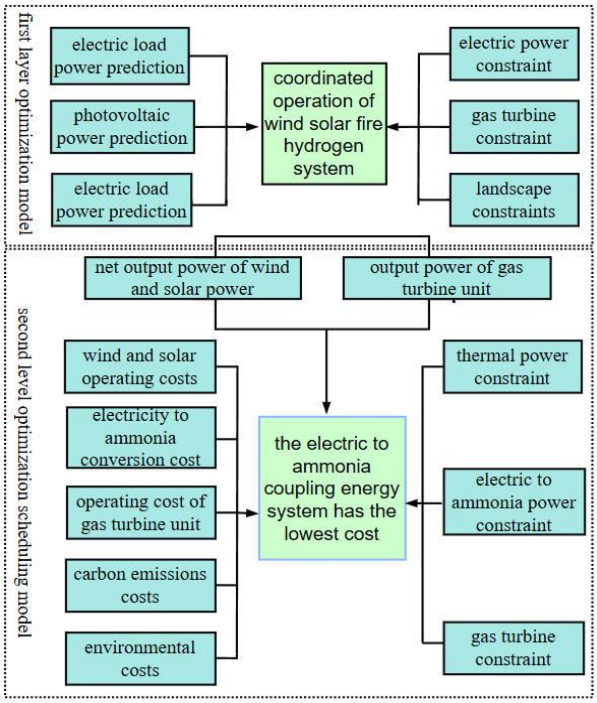


Fig. 2. dual-layer optimization model.

In this model, the upper layer prioritizes coordinated operation among microgrid components while incorporating performance metrics of the thermal-wind-solar-ammonia system. It assesses three critical aspects:power output performance of thermal power units,renewable accommodation capacity for wind and photovoltaic power generation,operational status of the integrated electrolytic hydrogen-to-ammonia production system,with primary focus on economic efficiency and operational stability.

First, this model uses μ as the output fluctuation coefficient of coal-fired units, calculated by equation (2). A smaller μ indicates more stable unit output. In this paper, coal-fired units include thermal power units and combined heat and power units.

$$\mu = \sum_{t=1}^{S} \left| p_t^{gt} - \overline{p}^{gt} \right| / (24 \overline{p}^{gt}) \tag{2}$$

In the formula, p_t^{gt} is the total output power of the coal-fired unit at each time interval t, and $\overline{p}^{gt}$ is the average output power during the operating time of the coal-fired unit.

Second, this paper considers the efficiency of coal-fired units, expressed by formula (3)[11,12]. When the output of formula (3) is closer to 1, the unit's actual power is closer to the rated value. This indicates lower coal consumption for power generation and improved operational stability and economic efficiency.

$$\varphi = \sum_{t=1}^{S} p_t^{gt} / (24 p_{max}^{gt}) \tag{3}$$

In the formula: p_{max}^{gt} is the theoretical maximum outputpower of the coal-fired unit.

Third, the instability of wind and solar photovoltaic generation can impact the entire system's stability. Therefore, this paper introduces an index called the renewable-energy-utilization ratio for power-to-ammonia, calculated by equation (4). Since the power-to-ammonia process has relatively low energy efficiency, a smaller value of this ratio means less wind and solar power is allocated to it. Consequently, more power can be used to directly satisfy the electrical load demand.

$$\delta = \sum_{t=1}^{S} p_t^{ele,ECA} / \sum_{t=1}^{S} (p_t^{wt,pre} + p_t^{pv,pre}) \tag{4}$$

In the formula: $p_t^{wt,pre}$is the wind and solar power used for power-to-ammonia in period t; $p_t^{pv,pre}$ is the predicted wind power in period t; $p_t^{ele,ECA}$ is the predicted solar photovoltaic power in period t.

Fourth, to comprehensively evaluate the output of coal-fired units, their utilization, and the proportion of renewable power

used in power-to-ammonia, this model constructs a dual-layer scheduling optimization index as shown in equation (5). This index reflects the integrated operation of thermal, wind, solar, and ammonia systems. A higher index value indicates better coordinated operation of the system's electrical components.

$$\omega = -0.33\mu + 0.39\varphi - 0.28\delta \tag{5}$$

In the formula, the weighting coefficients are calculated using the DEMATEL method from reference [13], which is designed for determining weights of macro-demand indicators (see Appendix A for details). Although reference differs in research context, the three indicators defined in this paper (output fluctuation coefficient of coal-fired units, utilization of coal-fired units, and proportion of renewable power for power-to- ammonia) are closely related to the safety, economic efficiency, and social benefit assessment of distribution networks.

Based on the heat load demand curve, this paper aims to minimize the operational cost of the entire system in the second-layer model, and optimally dispatches the system's power output. By calculating with the dual-layer optimization model, the optimal power generation schemes for all components and the minimal operational cost of the whole system can be determined.

3.2 First-Layer Scheduling Optimization Model

3.2.1 Model Objective Function

Considering equation (5), the objective function for the first-layer scheduling optimization model in this paper is set as equation (6). When this equation reaches its maximum value, it indicates the optimal coordinated operation of the thermal-wind-solar-ammonia system.

$$\max(-0.33\mu + 0.39\varphi - 0.28\delta) \tag{6}$$

3.2.2 Constraints

The first layer of the model is subject to the following constraints.

Power generation constraints of photovoltaic, wind-turbine, and coal-fired units in the first-layer model:

$$\begin{cases} 0 \le p_t^{wt,o} \le p_t^{wt,pre} \\ 0 \le p_t^{pv,o} \le p_t^{pv,pre} \\ p_{min}^{gt} \le p_t^{gt} \le p_{max}^{gt} \end{cases} \tag{7}$$

In the formula, $p_t^{wt,o}$ is the power output of wind power to meet the electric load demand at time t, $p_t^{pv,o}$ is the power output of photovoltaic at time t used to directly meet the electric load demand, and p_{min}^{gt} is the minimum power output of the coal-fired units in the system.

1)Constraints on curtailed wind and solar power.

To prevent excessive curtailment of wind and solar power during the optimization of the thermal-wind-solar-ammonia system's coordinated operation index, this paper, based on the "Clean Energy Consumption Action Plan (2018–2020)" [14], sets the maximum allowable curtailment limits as follows:

$$\begin{cases} \sum_{t=1}^{S} p_t^{wt,aq} / \sum_{t=1}^{S} p_t^{wt,pre} \le \varsigma_{max}^{wt} \\ \sum_{t=1}^{S} p_t^{pv,aq} / \sum_{t=1}^{S} p_t^{pv,pre} \le \varsigma_{max}^{pv} \end{cases} \tag{8}$$

In the formula: $p_t^{wt,aq}$ is the curtailed wind power, $p_t^{pv,aq}$ is the curtailed solar power; $\varsigma_{\max}^{wt}$ is the maximum allowable curtailment rate of wind power, which is 15%, $\varsigma_{\max}^{pv}$ is the maximum allowable curtailment rate of solar power, which is 10%.

2)Power constraints of wind and solar power used for power-to-ammonia in the first-layer model.

The operation efficiency of ammonia-synthesis technology depends on the installed wind-power capacity. The larger the capacity, the higher the efficiency, and vice versa. This paper assumes that the wind and solar power input to power-to-ammonia is over 50% of the equipment's capacity.

$$p_t^{ele,ECA} \ge 50\% p_{max}^{ECA} \tag{9}$$

In the formula: p_{max}^{ECA} is the maximum capacity of the power-to-ammonia equipment in the system.

3)Electric load balance constraints.

Electric load balance constraints must be satisfied at all times.

$$p_t^{wt,o} + p_t^{pv,o} + p_t^{gt,o} = p_t^{load} \tag{10}$$

In the formula, p_t^{load} is the electric load demand power at time t.

3.3 Second-Layer Scheduling Optimization Model

3.3.1 Model Objective Function

The second-layer model aims to minimize the total cost C of the power-to-ammonia integrated thermal-wind-solar system.

This cost covers wind power operation, coal-fired unit operation, curtailed wind and solar power, solar photovoltaic operation, power-to-ammonia operation, carbon emission, and environmental costs.

$$C = C_{wt} + C_{pv} + C_{aq} + C_{gt} + C_{ECA} + C_{co_2} + C_{en} \tag{11}$$

1) The second-layer model meets the costs of photovoltaic, wind power, and curtailed renewable energy.

$$\begin{cases} C_{wt} = c_{wt} \sum_{t=1}^{S} p_t^{wt} \\ C_{pv} = c_{pv} \sum_{t=1}^{S} p_t^{pv} \\ C_{aq} = c_{aq} \sum_{t=1}^{S} p_t^{aq} \end{cases} \tag{12}$$

In the formula: c_{pv} is the unit cost coefficient of photovoltaic power in the second-layer model; c_{wt} is the unit cost coefficient of wind power; c_{aq} is the unit cost coefficient of curtailed renewable energy; the actual outputs of photovoltaic and wind power at time t are $p_t^{pv}$and p_t^{wt} , respectively.

2) Operation costs of thermal power units and combined heat and power (CHP) units.

CHP units only participate in regular peak regulation, while thermal power units participate in both regular peak regulation (RPR) and deep peak regulation (DPR). But in practice, the ammonia produced by power-to-ammonia can't meet the actual demand of thermal power units. Therefore, only thermal power units are used for ammonia cofiring in this paper. Also, considering that the equipment maintenance cost of coal-fired units is ab-out 0.29% of the fuel cost [15], it's neglected in this model to simplify calculations.

The operation cost of thermal power units (including fuel and loss costs) and CHP units (only fuel costs) are calculated and summed up as the total operation cost of coal-fired units.

$$C_{gt} = C_{gt}^{tpu} + C_{gt}^{hscu} \tag{13}$$

Ammonia cofiring in thermal power units replaces some coal. Thus, the actual coal consumption of thermal power units is

$$m_t^{coal,gt} = a_1 p_t^{gt,gt^2} + b_1 p_t^{gt,gt} + c_1 + m_t^{NH_3} p_{NH_3} / p_{coal} \tag{14}$$

In the formula, a_1、b_1 and c_1 are the fuel consumption characteristic coefficients of the thermal power unit in the model. $p_t^{gt,gt}$is the power output of the unit during period t. $p_{NH_3}$and p_{coal} are the lower heating values of ammonia and coal, respectively. $m_t^{coal,gt}$ is the coal consumption of the unit during period t and $m_t^{NH_3}$ is the amount of ammonia cofired during period t.

Additionally, the ammonia cofiring ratio of the thermal power unit in the model during period t is defined as

$$r_t = m_t^{NH_3} p_{NH_3} / (m_t^{coal,gt} p_{coal}) \tag{15}$$

During the operation of thermal power units, rotor wear raises operating costs. In regular peak-regulation phases, this wear is negligible. However, during deep peak-regulation, excessive alternating thermal stresses on the rotor shaft cause low-cycle fatigue and creep damage to the unit, leading to significant costs. Deep peak-regulation is divided into two stages based on damage levels. The Manson-Coffin formula calculates the rotor's cyclic crack-initiation cycles $L(p_t^{gt,gt})$, and unit purchase costs are used to quantify the damage-related costs.

$$c_t^{loss,gt} = \begin{cases} 0, p_t^{gt,gt} \in p_t^{RPR} \\ c_u \alpha_1 / [2L(p_t^{gt,gt})], p_t^{gt,gt} \in p^{RPR_1} \\ c_u \alpha_2 / [2L(p_t^{gt,gt})], p_t^{gt,gt} \in p^{RPR_2} \end{cases} \tag{16}$$

In the formula, α_1 and α_2 are the damage coefficients for deep peak-regulation stages 1 and 2, respectively. $c_t^{loss,gt}$ represents the wear-and-tear cost of the thermal power unit, and c_u is the unit's cost per unit.

The operating cost of the thermal power unit is

$$C_{gt}^{tpu} = \sum_{t=1}^{S} (c_{coal} m_t^{coal,gt} + C_t^{loss,gt}) \tag{17}$$

Analysis In the formula, ccoal is the price of coal. For combined heat and power (CHP) units that burn coal, the main cost is coal:

$$m_t^{coal,hscu} = a_2 p_t^{gt,hscu^2} + a_2 d_{vl}^2 W_t^{gt,hscu^2} + 2a_2 d_{vl}^2 W_t^{gt,hscu} \cdot W_t^{gt,hscu} + b_2 p_t^{gt,hscu} + b_2 W_t^{gt,hscu} + c_2 \tag{18}$$

$$C_{gt}^{hscu} = c_{coal} \sum_{t=1}^{S} m_t^{coal,hscu} \tag{19}$$

In the formula, $m_t^{coal,hscu}$ is the coal consumption of the combined heat and power (CHP) unit at time t. a_2 , b_2 , c_2 , and d_{vl} are the unit's characteristic coefficients. $p^{gt,hscu}$ and $W^{gt,hscu}$ are the unit's electrical and thermal output powers at time t, respectively.

3) Levelized cost of energy calculation for the power-to-ammonia system.

In the model, hydrogen is supplied by water electrolysis and ammonia by pressure swing adsorption (PSA). The required

electricity comes from photovoltaic power generation and wind power generation. Since the ammonia-synthesis catalyst is durable, its cost is ignored. Thus, only water, the raw material, needs to be purchased externally.

$$C_{ECA} = C_{H_2o} + C_{equ,cost} \tag{20}$$

$$C_{H_2o} = c_{H_2o} \sum_{t=1}^{S} m_t^{H_2o} \tag{21}$$

In the formula, C_{H_2o} and $C_{equ,cost}$ are the water supply cost and O&M cost, respectively. c_{H_2o} is the water price parameter, and $m_t^{H_2o}$ is the water-consumption coefficient corresponding to the operating time t.

In this optimization model, the main costs lie in the electrolyzers for water splitting, ammonia-synthesis equipment, and nitrogen-generation devices.Proton-Exchange Membrane (PEM) water electrolysis, with its fast dynamic response and wide operating range, better suits renewable-energy-based hydrogen production.Thus, PEM with a hydrogen-production efficiency of about 67%[16] is chosen here. Studies indicate that for ammonia demand (typically under 3000m³/h) and given the intermittent renewable power supply for ammonia equipment[17], Pressure Swing Adsorption (PSA) is used in this model for ammonia production. As PSA ammonia equipment is low-cost, its maintenance cost is neglected. Therefore, equipment maintenance costs mainly come from the electrolyzers and ammonia- synthesis units.

$$C_{equ,cost} = c_{cost} \sum_{t=1}^{S} (p_t^{wt,ECA} + p_t^{pv,ECA}) \tag{22}$$

In the formula, c_{cost} is the unit-power O & M cost parameter of the wind-ammonia system within the computational framework. $p_t^{wt,ECA}$ is the cumulative energy-transmission parameter from the renewable energy supply to the ammonia-synthesis unit in period t. $p_t^{pv,ECA}$ is the total electricity-demand parameter of the electrolysis-based ammonia system in period t.
The production amounts of ammonia and nitrogen are as follows:

$$m_t^{ECA,NH_3} = (p_t^{wt,ECA} + p_t^{pv,ECA}) / n_{ECA} \tag{23}$$

$$m_t^{N_2} = (p_t^{wt,PSA} + p_t^{pv,PSA}) / n_{N_2} \tag{24}$$

In the formula: $p_t{}^{wt,PSA}$ is the wind-power-supplied electricity for PSA in period t, $p_t{}^{pv,PSA}$ is the solar-power-supplied electricity for PSA in period t. $m_t^{N_2}$ is the nitrogen-production mass in period t. n_{ECA} and n_{N_2} are the specific energy-consumption coefficient of the electrochemical ammonia-synthesis unit and the energy-intensity factor of the air-separation nitrogen-production unit, respectively.

4) Carbon Emission Cost.

After ammonia cofiring is introduced in coal-fired units, CO_2 emissions are reduced, with the reduction rate equaling the heat-value-based fuel substitution rate [18].Thus, the carbon emission cost can be expressed as [19]:

$$E = e_g \sum_{t=1}^{S} (p_t^{gt,gt} + p_t^{gt,hscu}) + e_h \sum_{t=1}^{S} (w_t^{gt,hscu}) \tag{25}$$

$$m_t^{CO_2} = q_{CO_2} (m_t^{coal,gt} + m_t^{coal,hscu}) \tag{26}$$

$$C_{CO_2} = c_p (E - \sum_{t=1}^{S} m_t^{CO_2}) \tag{27}$$

In the formula: $e_g$represents the carbon emission quota per unit of electricity; e_h denotes the carbon emission quota per unit of heat; $m_t^{CO_2}$ stands for the system's CO_2 emissions during period t; E is the carbon emission rights quota; c_p represents the penalty cost factor for the system's carbon emission quota; and q_{co_2} indicates the amount of CO_2 emitted per unit of coal consumed in the system.

5) Environmental Cost.

During the operation of thermal power units, sulfur dioxide and nitrogen oxides are emitted. Although ammonia cofiring may increase carbon oxides emissions,combustion staging and optimized combustion can effectively control them. Thus, this paper assumes that the nitrogen oxides emissions from ammonia-cofired thermal power units are the same as those from coal-only firing, and the emissions are calculated as [20]:

$$C_{en} = \sum_{t=1}^{S} \sum_{j=1}^{J} y [m_j (1 - \chi_j) m_t^{coal} / X_j] \tag{28}$$

In the formula, y is the effluent charge collection standard parameter.m_j is the emission intensity factor of pollutant j from coal-fired units. J is the number of taxable pollutants in the system.X_j is the pollution amount of the jth pollutant in the system.χ_j is the removal efficiency of the environmental protection device for the jth pollutant.

3.3.2 Constraints

1) Power balance constraints:

$$p_t^{gt,gt} + p_t^{gt,hscu} = p_t^{gt} \tag{29}$$

$$W_t^{gt,hscu} + W_t^{ECA} = W_t^{load} \tag{30}$$

In the formula, W_t^{load} is defined as the heat demand parameter of the heating network during operation period t.

2) Ammonia-Fuel Mixing Ratio Control Limits.

Given that different proportions of ammonia combusti-on in coal-fired units can destabilize the system, it is imperative to im pose restrictions on the ammonia cofiring ratio.

$$0 \le r_t \le r_{max} \tag{31}$$

In the formula, r_{max} is the maximum allowable proportion of ammonia cofiring. Research has shown that in a 1.2 MW experimental furnace, cofiring ammonia and coal was successfully achieved with a heat ratio of 20% [21]. Therefore, the maximum upper limit of the ammonia cofiring proportion is set at 20%.

3) Operating region constraints:

$$\begin{cases} p_t^{ECA} = p_t^{wt,ECA} + p_t^{wt,PSA} + p_t^{pv,ECA} + p_t^{pv,PSA} \\ p_{min}^{G,hscu} \le p_t^{gt,hscu} \le p_{max}^{G,hscu} - d_{vl} W_t^{gt,hscu} \\ W_t^{gt,hscu} \le W_{max}^{gt,hscu} \\ 50\% p_{max}^{ECA} \le p_t^{ECA} \le p_{max}^{ECA} \end{cases} \tag{32}$$

4) Ramp rate constraints of coal-fired units.

$$\begin{cases} -\Delta p_{max}^{gt,gt} \le p_t^{gt,gt} - p_{t-1}^{gt,gt} \le p_{max}^{gt,gt} \\ -\Delta p_{max}^{gt,hscu} \le p_t^{gt,hscu} - p_{t-1}^{gt,hscu} \le p_{max}^{gt,hscu} \\ -\Delta W_{max}^{gt,hscu} \le W_t^{gt,hscu} - W_{t-1}^{gt,hscu} \le W_{max}^{gt,hscu} \end{cases} \tag{33}$$

In the formula: $\Delta p_{max}^{gt,gt}$is the maximum ramping power of thermal power units in the system; $\Delta p_{max}^{gt,hscu}$ is the threshold of power change gradient on the generation side $\Delta W_{max}^{gt,hscu}$ is the maximum adjustment limit of heat power on the heat supply side.

$$\begin{cases} -20\% p_{max}^{ECA} \le p_t^{ECA} - p_{t-1}^{ECA} \le 10\% p_{max}^{ECA} \\ p_{t+1}^{ECA} = p_t^{ECA}, t \in [4i+1, 4i+3], i \in [0,5] \in Z \end{cases} \tag{34}$$

5) Ramp rate constraints of electrolysis-based ammonia-synthesis units.

When modeling the power-adjustment boundaries of renewable-energy-based ammonia systems, the dynamic stability boundaries of electrochemical synthesis units must be considered. The unit-time power change rate must not exceed 10% of the equipment-nameplate value. During scheduling, the maximum ramp rate is reduced to 20% of capacity. Also, production-rate adjustments are allowed only once every four hours.

$$\begin{cases} -20\% p_{max}^{ECA} \le p_t^{ECA} - p_{t-1}^{ECA} \le 10\% p_{max}^{ECA} \\ p_{t+1}^{ECA} = p_t^{ECA}, t \in [4i+1, 4i+3], i \in [0,5] \in Z \end{cases} \tag{34}$$

4 Case Study Analysis

The component configurations within the dual-layer optimization model studied in this paper are as follows: the installed capacity of the thermal power unit is 500MW,wind power generation is 600MW, and photovoltaic power generation is 210MW. The rated power output of the cogeneration unit under pure condensing mode is 220MW, and the rated power of the electric ammonia production system is 100MW.The minimum load rates for the thermal power unit under different operating modes are: 50% for Regular Peaking Regulation (RPR), 40% for Deep Peaking Regulation Level 1 (DPR1), and 30% for Deep Peaking Regulation Level 2 (DPR2). The minimum operating load thresholds for conventional generating units and the CHP system are set at 55%, 45%, and 35% respectively.The unit ramp rate characteristic curves and the coal consumption characteristic matrix are detailed in Appendix B. The core model parameter sets are fully listed in Appendix C[16,20].

The load, wind power, and photovoltaic power generation data used in the case study were sourced from a specific region in Ordos, Inner Mongolia. The dataset encompasses both winter and summer periods. During winter, daytime conditions typically feature persistent low temperatures punctuated by intermittent snowfall. Conversely, the summer period is characterized by prolonged sunshine interspersed with periodic precipitation. The respective data profiles are presented in Fig.3 and Fig.4.

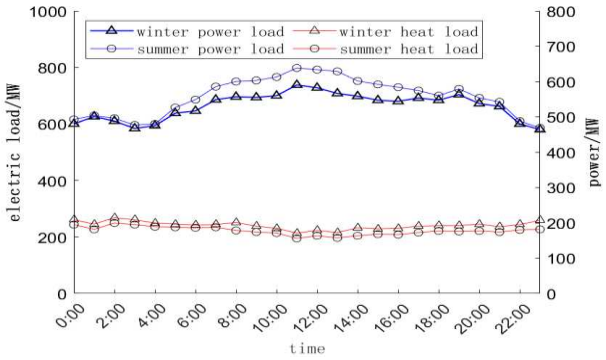


Fig. 3. Curve of Load

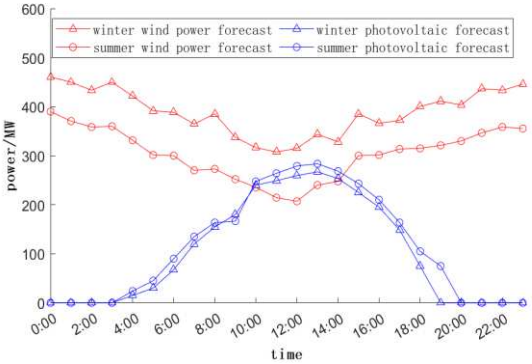


Fig. 4. Curve of Wind and solar power generation

4.1 Model Building

To analyze ammonia cofiring's economic and carbon-emission impacts on integrated energy systems, three models are designed for comparison:

Model 1: Only wind and solar power are considered, forming a thermal-wind-solar integrated energy system.All wind and solar power is fully utilized.

Model 2: This paper's dual-layer optimization scheduling strategy is applied to a thermal-wind-solar system without power-to-ammonia equipment.

Model 3: This paper's dual-layer optimization scheduling strategy is applied to a thermal-wind-solar system with power-to-ammonia equipment.

4.2 Analysis of Integrated Energy System Scheduling Results

This paper uses MatlabR2022b with the Cplex/YALMIP solver for optimization. The simulation period is 24 hours, with a 1-hour time step. The operational cost and carbon emissions of the model under different scenarios are shown in Table 1.

Table 1 Cost and carbon emissions under different daily scenarios in a certain area of ordos

scene	model	total cost /10^4 yuan	carbon emission/10t	Aband-oned wind rate%	abandoned light rate%
winter	1	513.25	9.29	0	0
	2	490.66	10.65	17.66	11.78
	3	483.43	10.15	2.27	0.97
summer	1	508.72	10.17	0	0
	2	481.18	11.07	15	10
	3	476.52	10.58	0.28	0.24

The results show that Model 2's cost is significantly reduced after applying the optimization model proposed in this paper. Model 3 further reduces the cost and also achieves lower carbon emissions compared to Model 2.

Taking the typical winter and summer days as examples, the analysis focuses on several aspects: the operation and curtailment costs of wind and solar power, the operation cost of gas-fired units, the operation cost of power-to-ammonia systems, carbon emission costs, environmental costs, and overall carbon emissions. As shown in Table 2, in winter, Model 2 sees a slight increase in carbon emission and environmental costs compared to Model 1, but other costs decrease significantly, with total costs dropping by 225,900 yuan (4.4%). This is because in Model 1, during deep peak-regulation, the low-load operation of coal-fired units reduces boiler efficiency and increases start-stop frequency, boosting equipment wear and tear. These technical constraints cause the coal-fired units' comprehensive cost to rise by 431,200 yuan compared to Model 2.

Table 2 Comparison of costs and carbon emissions of different models in a certain area of ordos

scene	model	total cost/10^4 yuan	wind and solar operation and abandoned wind and solar costs/10^4 yuan	operating cost of gas turbine unit/10^4 yuan	operating cost of electric to ammonia conversion /10^4 yuan	carbon emission cost/10^4 yuan	operating cost of electric to ammonia conversion/ 10^4 yuan	environmental cost/10^4 yuan	carbon emissions/ 10^3t
winter	1	513.25	34.31	461.26	0.00	13.14	0.00	4.52	9.29
	2	490.66	7.02	418.14	0.00	14.03	0.00	5.20	10.65
	3	483.43	37.18	422.37	6.67	12.13	6.67	5.08	10.15
summer	1	508.72	34.01	457.19	0.00	13.02	0.00	4.48	10.17
	2	481.18	6.88	410.06	0.00	13.76	0.00	5.10	11.07
	3	476.52	36.64	416.34	6.58	11.96	6.58	5.00	10.58

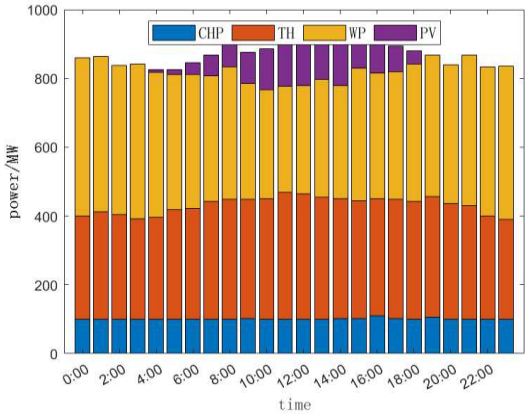
Compared to Model 2, Model 3 reduces total costs by 72,300 yuan (-1.47%). This cost reduction is driven by two factors: ammonia cofiring enables partial fuel replacement, and waste - heat recovery cuts coal consumption in the heating stage, creating a thermal-electrical decoupling synergistic optimization path. Moreover, Model 3 cuts carbon emissions by 0.5×10^3 tons compared to Model 2 (-4.69%), lowering carbon emission costs by 19,000 yuan (-13.54%).

In the summer scenario, Model 2 reduces total costs by 275,400 yuan (5.41%) compared to Model 1.

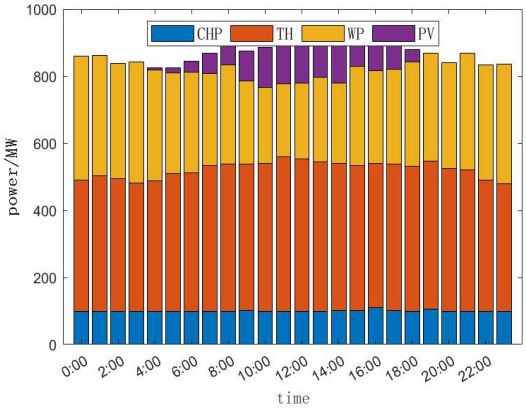
Model 3 further cuts costs by 46,600 yuan (0.97%) relative to Model 2. Carbon emissions and carbon emission costs decrease by 0.49×10^3 tons (4.43%) and 18,000 yuan (13.08%), respectively. Thus, integrating power-to-ammonia enhances the fire-wind-light system's low-carbon and economic performance.

The Fig.5 shows the winter power-scheduling results for Models 1-3. The model calculations indicate that combined heat and power (CHP) units have a higher power- generation cost than traditional coal-fired equipment.

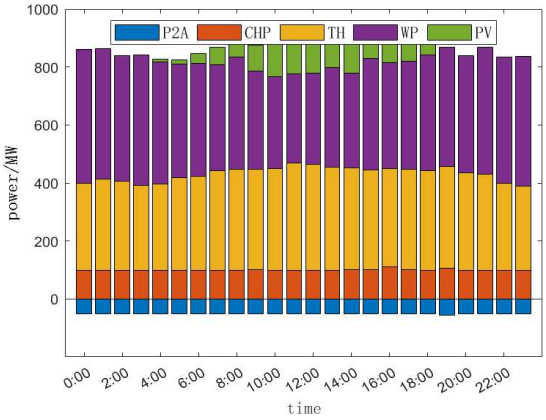
Increased Thus, under the dual-layer optimization framework, the second-layer scheduling system primarily adjusts conventional coal-fired units to ensure cost-effective system operation. Consequently, the analysis mainly centers on the output of coal-fired units.



(a)model1



(b) model2



(c) model3

Fig. 5 Power dispatch results

As shown in Fig.6, in Model 1, coal-fired units enter deep peak-regulation phases between 00:00-06:00 and 11:00-12:00 due to the full absorption of photovoltaic power generation and wind power generation. Model 2's scheduling shows two distinct phases: conventional peak regulation during 00:00-10:45 and 12:15-24:00, with deep peak regulation only around 11:00. Model 3, through a dual-layer optimization framework, keeps units in conventional peak-regulation throughout, eliminating deep peak-regulation needs and enhancing operational safety and stability. These results confirm the effectiveness of the proposed dual-layer scheduling model.

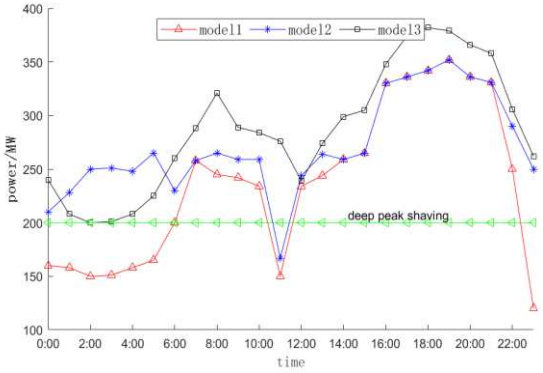
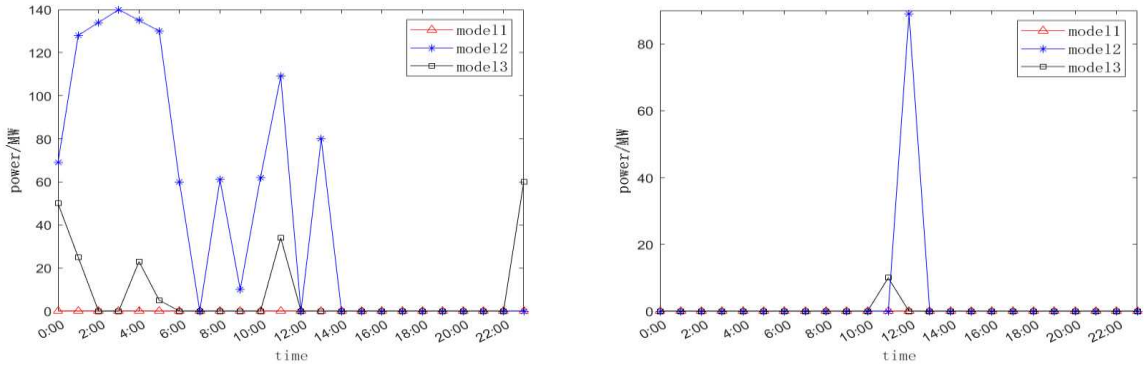


Fig.6 Output situation of thermal power units

The only drawback of the dual-layer scheduling optimization model is the curtailment of wind and solar power in Models 2 and 3. In Model 1, which prioritizes the full utilization of renewable energy, there is no such curtailment as wind and solar power are fully absorbed. Fig.7 allows for a comparative analysis of the curtailment situations among the three models.



(a)abandoned wind situation (b)abandoned light situation

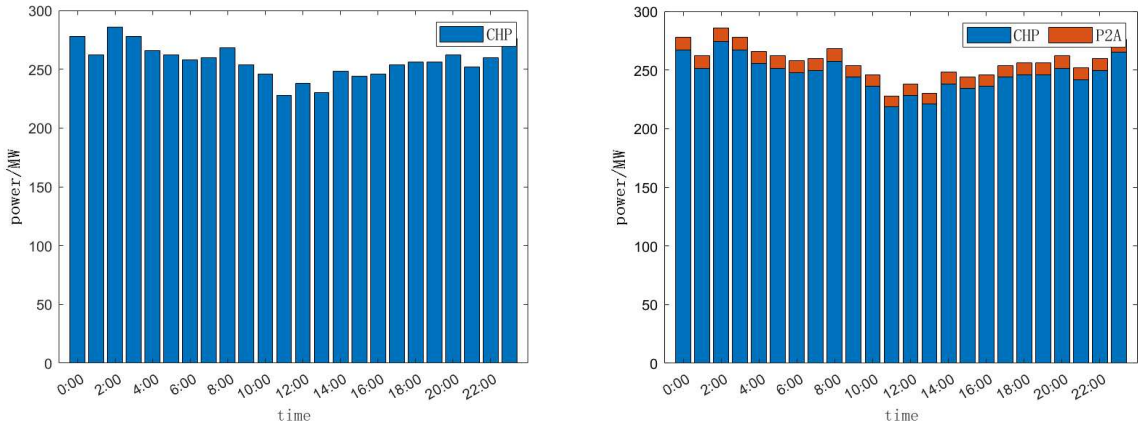
Fig.7 Abandoned energy situation

From Fig.7(a), Model 2 curtails wind power during the low-electricity-demand periods of 00:00-06:00 and 08:00-14:00. From Fig.7(b), it curtails solar power between 11:00 and 13:00, indicating renewable resource waste, with curtailment rates of 17.66% for wind and 11.78% for solar.

Model 3, incorporating power-to-ammonia, shows much better performance. It only curtails wind power between 00:00-01:00 and 04:00-05:00, and no solar power is curtailed between 10:00-12:00. The wind-power curtailment rate drops to 2.27%, and the solar-power curtailment rate to 0.97%. These results show that power-to-ammonia technology can effectively enhance the renewable-energy-accommodation capability of thermal-wind-solar systems.

Fig.8 shows the heat-scheduling results for Models 1-3. In the first two models, heat is supplied by combined heat and power (CHP) units. In Model 3, heat is also supplied by the heat generated during ammonia synthesis, which saves coal and reduces pollution. This demonstrates the power-to-ammonia system's significant economic and environmental benefits.

As shown in Fig.9, the techno-economics of the power-to-ammonia system can be quantified by its multi-energy-integration effect. Within the scheduling period, it can produce 91.2 tons of ammonia (equivalent to replacing 23.5 tons of standard coal) and simultaneously generate 76.8 MW·h of process waste heat (saving 9.3 tons of coal-firing for heat). Lifecycle cost calculations indicate that the system's coal-consumption intensity drops by 4.7 g/kWh, the marginal emission reduction cost decreases to 182 yuan/ton of CO_2, and the overall energy efficiency is significantly improved.



(a) model1 and model2 (b)model3

Fig.8 Thermal dispatch results

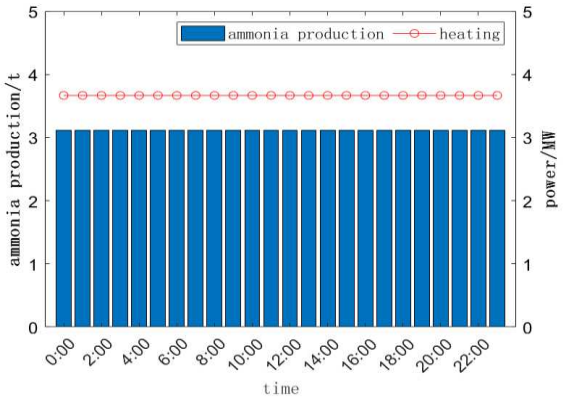


Fig.9 Ammonia production and heating situation from electric to ammonia conversion

5 Conclusions

This paper develops a dual-layer optimization model for a thermal-wind-solar integrated energy system with a power-to-ammonia unit. The model reduces operational and carbon-emission costs while improving the safety, stability, and renewable-energy-accommodation capacity of coal-fired units. Simulation results yield the following conclusions:

1. In typical winter and summer day scenarios in Ordos,Inner Mongolia, the model reduces system-operation costs by 4.4% and 5.41%, respectively.

2. After introducing power-to-ammonia technology and ammonia cofiring in coal-fired units, wind and solar curtailment is significantly reduced. Overall costs decrease, and carbon emissions drop by 4.69% and 4.43% in winter and summer scenarios, respectively. This dual optimization enhances both the economic and environmental performance of integrated energy systems.

Funding Statement: This study was supported by the State Grid Corporation of China's Science and Technology Project **4000-202455376A-3-2-HW**.

Conflicts of Interest: The authors declare that they have no conflicts of interest to report regarding the present study.

Reference

[1] ZHU Jianzhong , CUI Xiaobo , NI Weidong . Model predictive control based control strategy for battery energy storage system integrated power plant meeting deep load peak shaving demand[J] . Journal of Energy Storage, 2022, 46 : 103811 .

[2] Liu B ,Liu T ,Hu Z , et al.Short-term scheduling model for cascade diversion hydropower-wind-solar hybrid systems with Wasserstein-based distributionally robust chance constraints[J].Renewable Energy,2025,254123764-123764.

[3] CAREW N, WARNOCK W, BAYINDIR R, et al . Analysis of pumped hydroelectric energy storage for large-scale wind energy integration[J] . The International Journal of Electrical Engineering & Education, 2020 : 1-14 . doi: 10.1177/0020720920928456

[4] WANG Xuejie, ZHAO Huiru, LU Hao, et al . Decentralized coordinated operation model of VPP and P2H systems based on stochastic-bargaining game considering multiple uncertainties and carbon cost[J] . Applied Energy, 2022 , 312 : 118750 .

[5] BARTHELEMY H, WEBER M, BARBIER F . Hydrogen storage : Recent improvements and industrial perspectives [J] . International Journal of Hydrogen Energy, 2017, 42(11) : 7254-7262 .

[6] MORADI R, GROTH K M . Hydrogen storage and delivery: Review of the state of the art technologies and risk and reliability analysis[J] . International Journal of Hydrogen Energy, 2019, 44(23) : 12254-12269 .

[7] XU Da , ZHOU Bin , WU Qiuwei, et al . Integrated modelling and enhanced utilization of power-to-ammonia for high renewable penetrated multi-energy systems[J]. IEEE Transactions on Power Systems, 2020, 35(6): 4769-4780 .

[8] Liao F ,Ran R ,Zhang J .Construction and scheduling optimization of renewable energy consumption forecasting system for twisted tire porcelain manufacturing industry based on deep learning[J].Sustainable Energy Research,2025,12(1):27-27.

[9] CHEN Liang, WANG Chunbo, WANG Wenjing . Effect of ammonia co-firing on heat transfer , safety , and economy of coal-fired boilers[J] . Fuel, 2023, 334 : 126649 .

[10] ZHANG Guangming, WANG Wei, CHEN Zhenyu, et al . Modeling and optimal dispatch of a carbon-cycle integrated energy system for low-carbon and economic operation[J] . Energy, 2022, 240: 122795 .

[11] WANG Xi, LIU Fang, WANG Yunling, et al . Optimized dispatching based on wind-photovoltaic-hydropower-thermal-bundled strategy[J] . IOP Conference Series: Earth and Environmental Science, 2020, 467: 012038 .

[12] Hong C ,Ming C Y ,Xia J Y , et al.Comprehensive Evaluation Index System and Method of Smart Distribution Grid[J].Advanced Materials Research,2014,1070-1072(1070-1072):1339-1345.

[13] Hong C ,Ming C Y ,Xia J Y , et al.Comprehensive Evaluation Index System and Method of Smart Distribution Grid[J].Advanced Materials Research,2014,1070-1072(1070-1072):1339-1345.

[14] PALYS M J, KUZNETSOVA, TALLAKSEN J, et al . A novel system for ammonia-based sustainable energy and agriculture: Concept and design optimization[J] . Chemical Engineering and Processing-Process Intensification, 2019 , 140: 11-21.

[15] Hong C ,Ming C Y ,Xia J Y , et al.Comprehensive Evaluation Index System and Method of Smart Distribution Grid[J].Advanced Materials Research,2014,1070-1072(1070-1072):1339-1345.

[16] Purnamasari I ,Yerizam M ,Hasan A , et al.Oxygen Adsorption Kinetics Study used Pressure Swing Adsorber (PSA) for Nitrogen Production[J].Journal of Physics: Conference Series,2019,1167(1):012049 (7pp).

[17] Hong C ,Ming C Y ,Xia J Y , et al.Comprehensive Evaluation Index System and Method of Smart Distribution Grid[J].Advanced Materials Research,2014,1070-1072(1070-1072):1339-1345.

[18] Rowe K ,Cooke K ,Mokryani G , et al.A bi-level multi-node optimal siting, sizing, and operation of multi energy system in an integrated energy network of electricity-gas-heat with peer-to-peer trading[J].Applied Energy,2025,382125256-125256.

[19] Mingguang Z ,Weiqiang X ,Wenyuan Z .Combined optimal dispatching of wind-light-fire-storage considering electricity price response and uncertainty of wind and photovoltaic power[J].Energy Reports,2023,9(S1):790-798.

[20] Liu D ,Zang C ,Zeng P .Research on the optimal dispatch of wind power consumption based on combined heat and power with thermal energy storage[J].Energy Procedia,2018,152978-983.

[21] TAN Qinliang, DING Yihong, ZHENG Jin, et al . The effects of carbon emissions trading and renewable portfolio standards on the integrated wind-photovoltaic-thermal power-dispatching system: real case studies in China[J] . Energy, 2021, 222 : 119927 .

Appendix A

1）The interactions between the indices make objective assessment difficult. Below is a matrix scored by three experienced experts. They used a 1-9 scale to judge the direct influence between three indices empirically. The judgment sequence is descriptive.

$$\begin{bmatrix} 0 & 2 & 8 \\ 6 & 0 & 7 \\ 3 & 8 & 0 \end{bmatrix} \tag{A1}$$

2）Process the matrix from the expert scoring to get the direct-influence matrix in DEMATEL.

$$\begin{bmatrix} 0 & 1/4 & 1 \\ 3/4 & 0 & 7/8 \\ 3/8 & 1 & 0 \end{bmatrix} \tag{A2}$$

3）The influencing degree of (A2) is obtained as follows:

$$[3.6 \;\; 4.2 \;\; 3.0] \tag{A3}$$

4）The final weight values after normalizing the indices are as follows:

$$[0.33 \;\; 0.39 \;\; 0.28] \tag{A4}$$

Table B1 Parameters of thermal power unit

parameter	value
upper limit of power generation $P_{max}^{G,hscu}$ / MW	400
lower limit of power generation $P_{min}^{gt,gt}$ / MW	120
maximum allowable climbing power $\Delta P_{mx}^{gt,gt}$ /(MW·h)	150
a_i /(t·MW^{-2})	0.000 130 7
b_i /(t·MW^{-1})	0.232 22
c_i / t	16.007 26

Table B2 All parameters of combined-heat-and-power

parameter	value

Appendix B

upper limit of power generation $p_{max}^{G,hscu}$ / MW	212
lower limit of power generation $p_{min}^{G,hscu}$ / MW	100
upper limit of heating power $w_{max}^{gt,hscu}$ / MW	300
a_2 /(t · MW^{-2})	0.000 171 324
b_2 /(t · MW^{-1})	0.270 548 9
c_2 / t	11.537 43
c_{v1}	0.21
maximum allowable climbing power for power supply $\Delta p_{max}^{gt,hscu}$ /(MW · h)	60
maximum allowable climbing power for heating $\Delta w_{max}^{gt,hscu}$ /(MW · h)	60

Table 1 Main parameters in the model

parameters and units	value
heat release ratio used for heating in ammonia plants η^{ECA}	0.85
generate the heat power released by unit NH3 $\sigma/(MW\cdot h\cdot t^{-1})$	1.6044
unit cost coefficient of wind power $c_{wt}/[yuan\cdot(kW\cdot h)^{-1}]$	0.03
unit cost coefficient of photovoltaics $c_{pv}[yuan\cdot(kW\cdot h)^{-1}]$	0.04
bandoned unit cost coefficient for wind and solar power $c_{aq}/[yuan\cdot(kW\cdot h)^{-1}]$	0.15
low calorific value of ammonia $p_{NH_3}/(kJ\cdot kg^{-1})$	18720
low calorific value of coal $p_{coal}/(kJ\cdot kg^{-1})$	23022
unit price of coal $c_{coal}/(yuan\cdot t^{-1})$	1000
unit price of water $c_{H_2O}/(yuan\cdot t^{-1})$	5
the operating loss coefficient α_1 of stage DPR1	1.2
the operating loss coefficient α_2 of stage DPR2	1.5
unit cost of the crew/(yuan·kW-1)	3464
unit power maintenance cost of electric to ammonia equipment $c_{cost}/[yuan\cdot(MW\cdot h)^{-1}]$	46.48
unit energy consumption for PSA nitrogen production $n_{N_2}/[(MW\cdot h)\cdot t^{-1}]$	0.8
PSA collaborative ammonia production unit energy consumption $n_{ECA}/[(MW\cdot h)\cdot t^{-1}]$	11.49
carbon emission quotas for power supply units $e_g/[t\cdot(MW\cdot h^{-1})]$	0.69135
carbon emission quota for heating units $e_h/[t\cdot(MW\cdot h^{-1})]$	0.3
CO_2 emissions per unit of coal-fired combustion $q_{co_2}/(t\cdot t^{-1})$	2.57
cost coefficient of carbon emission quota punishment $c_p/(yuan\cdot t^{-1})$	100
tax payable per pollution equivalent $y/(yuan\cdot kg^{-1})$	5
mass of SO_2 produced by unit coal combustion $m_{so_2}/(kg\cdot t^{-1})$	8.5
mass of NOx generated by unit coal combustion $m_{NO_x}/(kg\cdot t^{-1})$	7.4
efficiency of SO_2 removal by environmental protection devices $\eta_{so_2}/\%$	85
efficiency of environmental protection devices in removing NOx $\eta_{NO_x}/\%$	85
pollution equivalent of SO_2 G_{so_2}/kg	0.95
NOx pollution equivalent number G_{NO_2}/kg	0.95

Appendix C